# Optoelectronic-based pose sensing for a hand rehabilitation exoskeleton continuous structure

Bo He, Min Li, Renghao Liang, Ziting Liang, Wei Yao, Sina Sareh, Jun Xie, Guanghua Xu, and Yohan Noh

***Abstract*—Hand exoskeleton pose monitoring is of great importance in the rehabilitation training of stroke patients to ensure precise robotic trajectory control and provide a patient recovery assessment mechanism. In this paper, a low-cost pose sensor unit based on the principle of photoelectric reflection is proposed to measure the pose of a multi-segment continuous structure in a hand rehabilitation exoskeleton. The sensor unit consists of five photosensitive elements that measure the rotation angle of an arrangement of adjacent segments, each integrated with a sensing element, to estimate the actuator's motion. An accurate device with a user-friendly interface is then designed for calibration of the sensing elements. The experimental results indicate that the sensitivity exceeds 0.047 V/° for the sensing elements, and hysteresis and repeatability errors are less than 1.1% and 1.8%, respectively. A comparison between the proposed sensor output and the results benchmarked by a VICON motion capture system demonstrates that the sensor can measure the bending angle of the multi-segment structure with a mean error of 3.23 degrees.

Photosensitive element — Mirror — Multi-segment continuous structure shown in purple
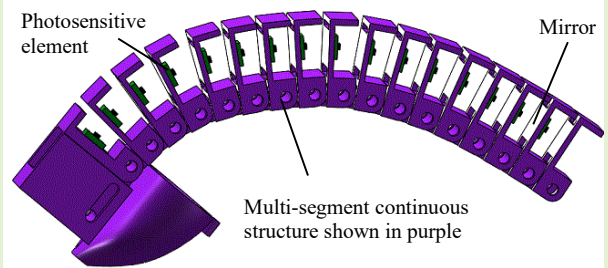
***Index Terms*—Optoelectronic sensors, Pose sensing, Infrared sensors, Hand rehabilitation exoskeleton**

I. Introduction

STROKE survivors often suffer from hand dysfunction that drastically inhibits their daily living activities [1, 2]. Repetitive motion exercises are considered an effective rehabilitation method for patients with post-stroke hand function impairments [3]. This method usually requires one-on-one interaction with a professional who assists and encourages the patient to perform the exercises. However, physical therapy involving professionals can be labor-intensive, time-consuming, and costly. Robotic rehabilitation devices have been introduced to solve these problems. Studies have shown that conducting intense, repetitive movements with the assistance of robots can significantly improve patients' hand motor functions [2].

Hand exoskeleton devices have drawn significant research attention in recent years and obtained promising research results [1]. Due to the safety issue of possible misalignment between the human finger joints and those of an exoskeleton with a rigid mechanical design during rehabilitation movements, flexible hand exoskeletons have become a popular research direction. In our previous research, we proposed a hand exoskeleton using a rigid-soft combined multi-segment structure [4]. The inherent features of this multi-segment structure eliminated the issue of joint misalignment between the device and the human finger, enhancing the simplicity and flexibility of the device. Moreover, its intrinsic compliance ensured that the hand exoskeleton was safe for human-robotic interaction.

The rehabilitation of motor function is greatly influenced by the sensorimotor experience [1] which aims to restore normal movements via rehabilitation training [5]. To enable this, a hand exoskeleton is required to help the patient conduct hand movements with normal motion patterns and requires precise trajectory control of the robot. Pose monitoring is essential for such closed-loop control of flexible hand exoskeletons. Additionally, pose monitoring could assist in denoting the patient's condition during rehabilitation training, evaluating the effectiveness of rehabilitation, and promptly adjusting the rehabilitation program to refine the rehabilitation exercise [6, 7].

Possible pose monitoring solutions for flexible hand exoskeletons include computer vision-based motion tracking, optical fiber sensors, electromagnetic sensors, flexible strain sensors, and photoelectric sensors. Computer vision-based motion tracking devices such as the VICON system (VICON Motion Systems Ltd, UK) [8], the Motion Analysis System (Motion Analysis Corp., Santa Rosa, CA, USA) [9, 10], Leap Motion (Leap Co., USA) [11, 12], and the Microsoft Kinect (Microsoft Corporation, Albuquerque, New Mexico，USA) [13, 14], have been designed to capture the 3D pose of the human

Bo He, Min Li, Renghao Liang, Ziting Liang, Jun Xie and Guanghua Xu are with the Department of Mechanical Engineering, Xi'an Jiaotong University, Xi'an 710049, China; Wei Yao is now with the Department of Biomedical Engineering, University of Strathclyde, Glasgow G4 0NW, UK; Sina Sareh is now with the RCA Robotics Laboratory, Royal College of Art, London SW7 2EU, UK; Yohan Noh is now with the Department of Mechanical and Aerospace Engineering, Brunel University London, Uxbridge UB8 3PH, UK.
Corresponding author: Min Li (e-mail: min.li@mail.xjtu.edu.cn) and Yohan Noh (e-mail: yohan.noh@brunel.ac.uk).

body. The conspicuous advantage of the vision-based method is its ability to capture the motion of human joints with remarkable precision and stability. However, this method requires additional devices and/or markers attached to the flexible hand exoskeletons to track their precise positions/orientations, and the consecutive hand motions tracked by a camera or a motion-tracking device may be undetectable when it is blocked by an object, causing recognition error. Further, this approach has a serious portability issue as the tracking device must always be placed near the flexible hand exoskeletons to carry out pose monitoring. Therefore, pose monitoring based on computer vision has a limited capacity for integration into flexible hand exoskeletons [11, 13].

Shape sensing using optical fibers has drawn significant research attention because they can be woven into objects that fit tightly into various surfaces and shapes. Optical fiber sensors using a macro-bending loss mechanism [15, 16], reflected light intensity modulation [17, 18], and Fiber Bragg Gratings (FBG) [19-21] have been used for pose sensing in soft robots. However, macro-bending of the fiber would lead to degradation of the fiber materials over time and require recalibration or replacement of fibers, and the measurement results depend heavily on the arrangement of the fibers. Regarding the FBG-based sensors, a costly interrogator is required for measuring wavelength. This method ensures high resolution of the measured data and can facilitate the miniaturization of a hand rehabilitation exoskeleton. However, the fabrication process is highly complicated because attaching an optical fiber (on which the FBG is mounted) in a soft structure is generally carried out by hand, and thermal drift must be compensated by adding a dummy FBG, meaning the overall manufacturing cost very expensive [22]. The principle of light intensity modulation is simple and guarantees stable light intensity signals at the fastest sampling rate. The problem of this approach is that many optical fibers may be required for measuring complicated shapes compared to simple shapes with constant curvature, making it difficult to miniaturize the overall size of many soft manipulators or applications [23].

Similar to computer vision-based motion capture systems, electromagnetic-based motion capture systems require additional devices such as electromagnetic generators and receivers, and are more frequently employed in stable environments like laboratories [24-26] because metal or any electronic devices creating a magnetic field could decrease the accuracy of motion capture information. The same portability issue as mentioned above is also encountered [24].

Flexible strain sensors can be mounted on the skin and change shape with human activities. The most widely implemented and practical flexible strain sensors are resistive-type sensors and capacitive-type sensors [27-31]. Resistive-type sensors are comprised of electrically conducting fillers and flexible insulating materials [28, 30]. Capacitive-type sensors always include two electrodes and a compliant insulating layer [31]. These sensors transduce human pose variation into electrical output signals with high flexibility, stretchability and easy-to-read circuitry [28]. However, in order to obtain high sensitivity, the strain sensor must have a large stretch range. This will negatively affect the life of the sensor [31]. Additionally, the strain sensor is not effective for monitoring

different shapes.

Another possible solution for shape sensing is the photoelectric sensing method. This sensing element has the advantages of low energy consumption and low noise. Several successful studies using the optoelectronic sensor have been reported for sensing shape information. Benjamin et al. employed three photoelectric sensing elements (QRE1113, Fairchild Semiconductor Corp.) to estimate the shape of a snake-like flexible manipulator [32], and Dalia et al. integrated them into the joints of a robot hand finger to measure its shapes [33]. In the former case, although the concept and idea were novel, the pose sensing accuracy was not precisely guaranteed. In the latter case, the proposed sensing method was not able to sense a large range of rotary position measurement. Moreover, the size of the used photoelectric sensing element was quite large, limiting further miniaturization of the overall size of pose sensing applications. Therefore, the sensing element would not be suitable for the multi-segment mechanism applied to our hand exoskeleton (see Fig. 1(a)). Using a light emitting diode (LED) and a photodiode, Dobrzynski et al. developed a deflection sensor to detect the shape of soft robots [34]. This approach allowed the LED and the photodiode to be placed separately on the robot, substantially reducing the impact on the
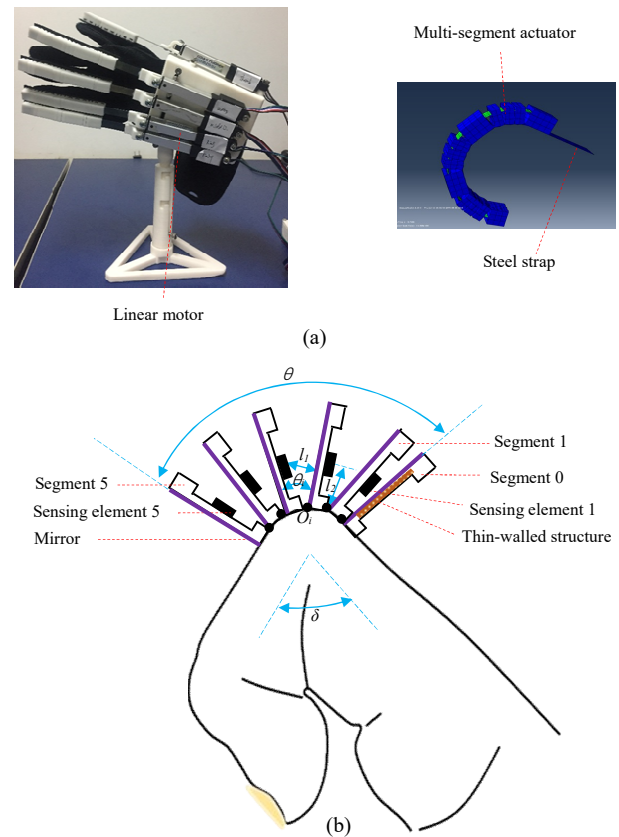

(a)

(b)

FIGURE 1.   **Shape sensor assembled into a multi-segment actuator in a hand rehabilitation exoskeleton: (a) exoskeleton for functional rehabilitation of the hand with multi-segment structure [4], and (b) overview of the photoelectric sensor for measuring the bending angle of the PIPJ actuator. In the figure, δ represents the rotation angle of PIP, θ represents the actuator rotation angle, θ_i represents the rotation angle between segment i and segment $i-1$, O_i represents the rotation center of segments i, l_1 is the distance between the sensing element surface and the mirror, and l_2 is the distance between the sensing element and the rotation center.**

robot's movement. However, additional conditioning circuitry or data correction was necessary because ambient light could affect the accurate measurement of the sensor. For the small actuator shown in Fig. 1(a), more compact sensing elements and simpler circuits should be utilized to improve assembly on the thin segment.

In this paper, we propose a miniaturized pose sensor unit using tiny photoelectric sensing elements and simpler circuitry. With these small sensing elements, the sensor has the potential to be miniaturized and integrated into a multi-segment continuous actuator to measure any complicated pose on the hand rehabilitation exoskeleton, as shown in Fig. 1(a) [4]. This paper presents the following contributions:

1) A low-cost and potentially miniaturized shape sensor is proposed and verified, which can detect different bending curvatures of multi-segment continuous structures;

2) An easy-to-install device is developed for precise calibration of the sensing elements after being integrated into the multi-segment continuous actuator.

In the remainder of the paper, Section II describes the design concept, and Section III presents the process of sensor parameter determination. Finally, in Section IV, the calibration and testing are described and the respective results are presented.

II. DESIGN OF THE SENSOR

A. Design Requirements

In this paper, the shape sensor unit is composed of a few reflective photoelectric sensing elements and then integrated into individual segments of the multi-segment structure in the proximal interphalangeal joint (PIPJ) of our previously presented exoskeleton [4]. The requirements listed below are considered in the sensor design.

1) To enhance the fit of the actuator with the hand during the rehabilitation movements, the segments should be as thin as possible. The thickness of the segment in our design is 5 mm. Therefore, the thickness of the sensing element should be negligible.

2) The sensing elements should be sufficiently compact so that the miniaturized shape sensor unit can be integrated suitably with the actuators within the respective size limits and do not impose mechanical restrictions on the normal hand motions.

3) The sensing elements should be low-cost, easy to fabricate, reliable, and able to be produced at scale.

4) The conditioning circuit of the pose sensor unit should not be complex or heavy; without the need for other post-processing electronic components such as amplifiers. This facilitates integration and low noise measurements.

5) The mean error should be less than 5° for the reliable evaluation of movement impairments in clinical contexts, as explained in [35].

B. Sensing Principle And Configuration of The Sensor Unit

As illustrated in Fig. 1(b), the actuator corresponding to the PIPJ is composed of six segments. Segment i rotates around point O_i relative to segment i-1, $i \in [1, 5]$, and five sensing elements are attached to five segments numbered 1–5. Additionally, θ_i represents the rotation angle of the segment i measured by the sensing element i. Thus the angle of the

actuator rotation θ can be calculated by (1). The rotation angle of the PIPJ (δ) is approximately 180° minus θ.

$$\theta = \sum \theta_i, \ i \in [1, 5] \tag{1}$$

To detect θ_i, a surface-mount device (SMD) chip reflective photoelectric sensing element (NJL5901R-2, New Japan Radio Co., Ltd. Tokyo, Japan) is employed. This sensing element has the following advantages. First, the small size (1.0 mm * 1.4 mm * 0.6 mm) makes it possible to design a compact sensor that can be integrated into a small, flexible mechanical structure. Secondly, the price of each sensing element is only around $0.20, making it feasible to form a shape sensor unit consisting of multiple sensing elements at a low cost. The relatively high stability, high sensitivity, magnetic/electrical noise immunity, and absence of additional electronic filtering are further reasons why we use this reflective photoelectric sensing element.

The measurement principle of the sensing elements is adopted to detect θ_i, as shown in Fig. 2(b). The sensing element consists of a LED and a phototransistor, which are packaged together in a chip. The total power dissipation is 60 m W, and a 5 V direct-current power supply is employed to power them. The infrared signal from the LED is reflected by a mirror, and a phototransistor collects part of the reflective optical signal, eventually converting the reflected light intensity into the output voltages. Changing the distance d between the mirror and the sensing element surface modulates the intensity of the reflective optical signal received by the phototransistor. The sensing element outputs a voltage u_i of 0–5 V depending on the light intensity. Therefore, the distance d can be represented reliably by the output voltage. In our design, the distance l_1 (shown in Fig. 1(b)) between the sensing element surface and the mirror changes during the rotation of the adjacent segments, resulting in a change in the light intensity received by the photoelectric as well as the output voltage of the sensing element. Consequently, the rotation angle of the adjacent segments θ_i can be calculated by the output voltage.

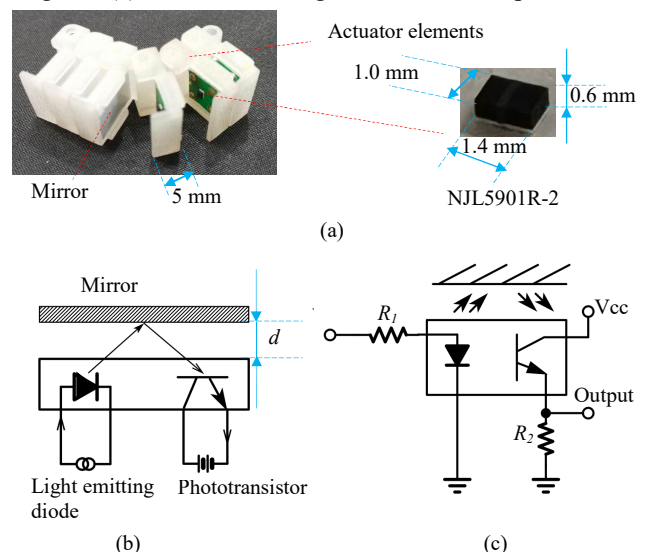Figure 2(a) shows the configuration of the shape sensor unit

FIGURE 2. **(a) Configuration of shape sensor mounted on the multi-segment actuator (left) and reflective photoelectric sensor NJL5901R-2 (right); (b) sensing principle; (c) circuit diagram of sensing elements. In the figure, *d* represents the distance between the mirror and the surface of sensing elements.**

mounted on the multi-segment structure. The sensing elements are soldered on the printed circuit board (PCB) by surface-mount technology to ensure precise implementation. Five PCBs with chip reflective photoelectric sensing elements are individually installed on one side of the compact segment. A reflective sheet made from 3M™ Engineer Grade Reflective Sheeting 3200 (3M, Sao Paulo, USA) is taped to the other side of each block to play the role of a diffuse mirror. This material can be easily cut to the desired shape with scissors and has no risk of breakage.

The rotation angle between adjacent segments θ_i can be accurately measured based on the sensing principle. The configuration described above and the rotation angle of the actuator corresponding to the PIPJ joint can be calculated by (1).

III. SENSOR UNIT PARAMETER DETERMINATION

As shown in Fig. 2(c), the measurement circuit consists of a sensing element (NJL5901R-2), two resistors that are cited as R_1 and R_2, and a 5 V direct-current power supply. R_1 is in series in a circuit containing the LED, which acts as a current limit to protect the LED. R_2 is in series in a circuit containing the phototransistor, which converts current into voltage. The relationship between input light intensity and output voltage changes when the combination of R_1 and R_2 with different resistance values is selected. This section aims to experimentally investigate the effect of R_1 and R_2 on the static characteristics and to determine the optimal combination of R_1 and R_2 to achieve the appropriate performance of the target sensor unit. To analyze the characteristics accurately, the target measurement angle is converted into displacement. The experimental setup shown in Fig. 3 is used for analyzing the input and output characteristics with different combinations of R_1 and R_2.

The desired displacement measurement range of the sensing elements is first estimated. As shown in Fig. 1(b), the distance l_2 between the sensing element and the center of rotation is 6 mm. The distance l_1 is calculated by the following equation.

$$l_1 = l_2 * \tan\theta_i \qquad (2)$$

The rotation angle of θ_i is less than 50° during the actuator operations. Therefore, the displacement l_1 should be greater than 7.2 mm according to Equation 2. The input-output characteristic curve within the displacement range of 10 mm is set to the analysis target for the following two reasons: first, the mirror cannot stay parallel to the sensing element surface during the movement, resulting in the loss of additional light intensity; second, the dead zone shown in Fig. 4(a) cannot be used to measure the displacement. In our application, the length of the dead zone is used to determine the distance between the sensing element surface and the mirror at the initial position. This design protects the sensor surface and the mirror because they do not touch each other during the measurement process.

As shown in Fig. 3, the experimental platform includes a power supply, a stepper motor with a ball screw, an Arduino MEGA 2560, a breadboard and a computer. The power supply (Agilent U8002A, Keysight Technologies, Santa Rosa, CA) provides 12 V direct voltage to the stepper motor. The Arduino
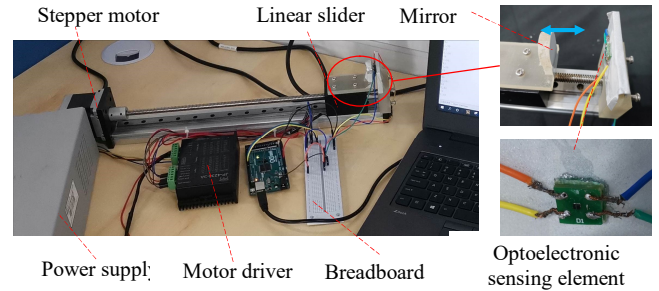

FIGURE 3. **Experiment setup for exploring the relationship between input displacement and output voltage under different combinations of R_1 and R_2.**

MEGA 2560 plays the role of controlling motor movement, providing 5 V direct voltage to the sensing element, and collecting data. The photoelectric sensing element is fixed to the stepper motor base, and the mirror is affixed to a linear slider, which can be guided by the ball screw to be closer to or further away from the surface of the sensing element while remaining parallel to it. Different resistance pairs are quickly replaced using the breadboard in order to verify the influence of the resistances on the sensor characteristics.

At the beginning of the experiment, the mirror is aligned with the surface of the sensing element by moving the linear slider on the linear motion unit, and this position is marked as ground zero. At ground zero, the distance between the sensing element surface and the mirror is zero. The stepper motor is controlled to drive the mirror away from the sensing element in the range of 10 mm (forward trial), and then return to the ground zero (backward trial). During this process, the output voltage for each 0.1mm movement of the mirror is recorded. The following sets of values for R_1 and R_2 are used during the test: R_1= {0.25, 0.5, 1, 2, 3, and 4 k Ω}, R_2= {1, 5, 10, 15, 20, 25, 30, 40, and 50 k Ω}. Each combination of the resistors is used in five test iterations.

Fig. 4 illustrates that the relationships between the output voltage and the input displacement are distinct for different combinations of R_1 and R_2. This result proves that the output characteristics can be adjusted by modifying the resistance values of R_1 and R_2. Each subgraph shows the effect of different R_2 on the characteristics when R_1 remains at a certain resistance value. According to the charts, when R_2 is increased, the dead zone increases significantly. The smaller the resistance value of R_1, the more obvious the effect of R_2 on the dead zone. In addition, the output range from trough to stable value is positively correlated with values of R_2. The curves in the same line type among different subgraphs represent the influence on the output characteristics with varied values of R_1 when R_2 is fixed. The results demonstrate that the rise of R_1 could bring about growth in the starting voltage of the sensing elements and a faster speed to reach the peak. In addition, the ratio of R_2/R_1 is a critical factor affecting the sensor performance. A low ratio indicates a small dead zone, a faster speed to reach the peak, and a small measurement range. Thus, the low ratio should be considered when tiny displacements must be measured at a high resolution.

In our application, the thickness of the segment (Fig. 2(a), left), the PCB, the sensing element (Fig. 2(a), right), and the thin-walled structure (Fig. 1(b)) are 5, 0.8, 0.6, and 1.5 mm, respectively. Therefore, the length of the dead zone in our design should be smaller than 2.1 mm (5 – 0.8 – 0.6 – 1.5 = 2.1
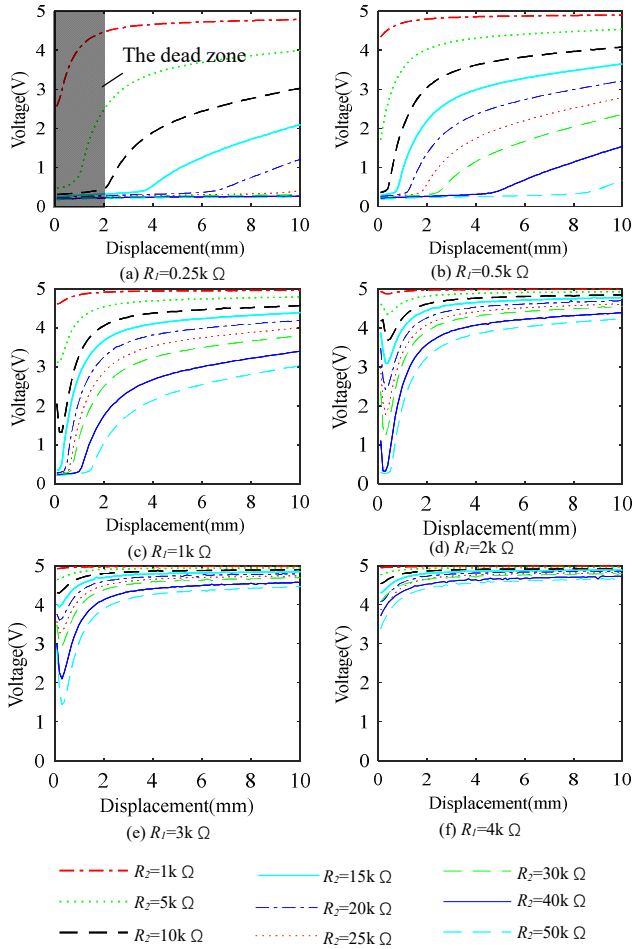
FIGURE 4. **The relationships between the output voltage and the input displacement under different combinations of R_1 and R_2. The shaded portion of subfigure (a) indicates the dead zone when R_1 is 0.25 k Ω, and R_2 is 10 k Ω.**

FIGURE 5. **(a) The relationship between the input displacement and the output voltage of the sensing element when R_1 is 0.25 k Ω and R_2 is 10 k Ω. Forward trial refers to the process of keeping the mirror away from the sensing element, and backward trial refers to the process of the mirror approaching the sensing element; (b) Larger view of the location marked by the blue rectangle.**

mm). Based on the analysis at the beginning of Section III, the length of the sensing area should be greater than 7.2 mm. Under the above conditions, we searched for the two resistors that enabled the sensing elements to measure with good linearity and resolution in the range of 2–10 mm. Eventually, the combination of 0.25 k Ω and 10 k Ω for R_1 and R_2 was selected to measure a displacement target of 10 mm. The input and output characteristics of this sensing element within the range of 2 and 10 mm are illustrated in Fig. 5. The experimental results show a hysteresis error of 4.1%, a repeatability error of 0.78%, an average sensitivity of 0.32 V/mm on the forward trial, and an average sensitivity of 0.33 V/mm on the backward trial within the range of 2 to 10 mm. The same experimental setup was employed to verify the durability of the sensor element. The results suggested that the input and output characteristics of the sensor remained constant after ten thousand cycles in principle.

IV. SENSOR CALIBRATION AND TESTING

The experiment result of the photoelectric sensing element in Fig. 5 shows the measurable distance range by optimizing two resistors is R_1=0.25 k Ω and R_2=10 k Ω. However, when the photoelectric sensing element is mounted on the multi-segment actuator, as shown in Fig. 2 (top), the characteristic curve
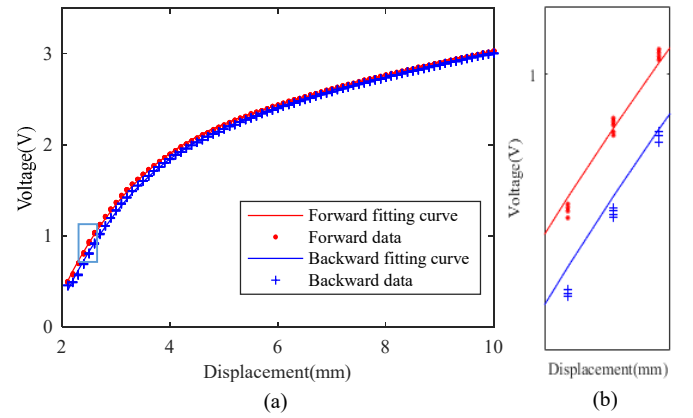
representing the relationship between a distance and a voltage would not be the same as Fig. 5as the mirror cannot stay parallel to the sensing element surface during the movement. Additionally, depending on the methods used to affix the mirror on the multi-segment actuator (Fig. 2) and mount the photoelectric sensing element there, each characteristic curve of the photoelectric sensing elements assembled into the multi-segment actuator would be slightly inconsistent. Therefore, the five assembled sensing elements were calibrated separately to determine their respective input and output equations. Subsequently the effectiveness of the sensing unit composed of the five sensing elements was verified by comparing the actuator motion angle measured by the designed sensing element against the rotation angle of the PIPJ of a wooden hand model gauged by the VICON T40S capture system.

Section IV A describes a calibration device for calibrating the relationship between the input rotation of the adjacent segments and the output voltage of the sensing element. Based on the relationship, the sensor is able to measure the rotation angle, although the mirror is not parallel to the sensing element surface. The device can also be applied to correct the sensor parameters after a period to improve its measurement accuracy and prolong its service life. Section IV B depicts the calibration experiment and the results of the five sensing elements.

A. Calibration Device

As shown in Fig. 6, the calibration device consists of five main components (MC_1, MC_2, MC_3, MC_4, and MC_5). MC_1 is a support structure to hold the device stably on the stepper motor; MC_2 is a fan-shaped part of radius r that can rotate around a center (O_1) driven by a wire attached to MC_3; MC_3 is screwed on the linear slider to achieve precise movement control of the wire as shown in Fig. 6; MC_4 is screwed to MC_1 and locks the segments numbered 1 to i, $i \in [1, 5]$; MC_5 locks the segments numbered $i + 1$ to 6 and makes them rotate around O_i (see Fig. 1(b)) driven by MC_2. We employ bearings to reduce friction during rotation. MC_4 and MC_5 are designed according to the construction of the multi-segment structure, allowing the
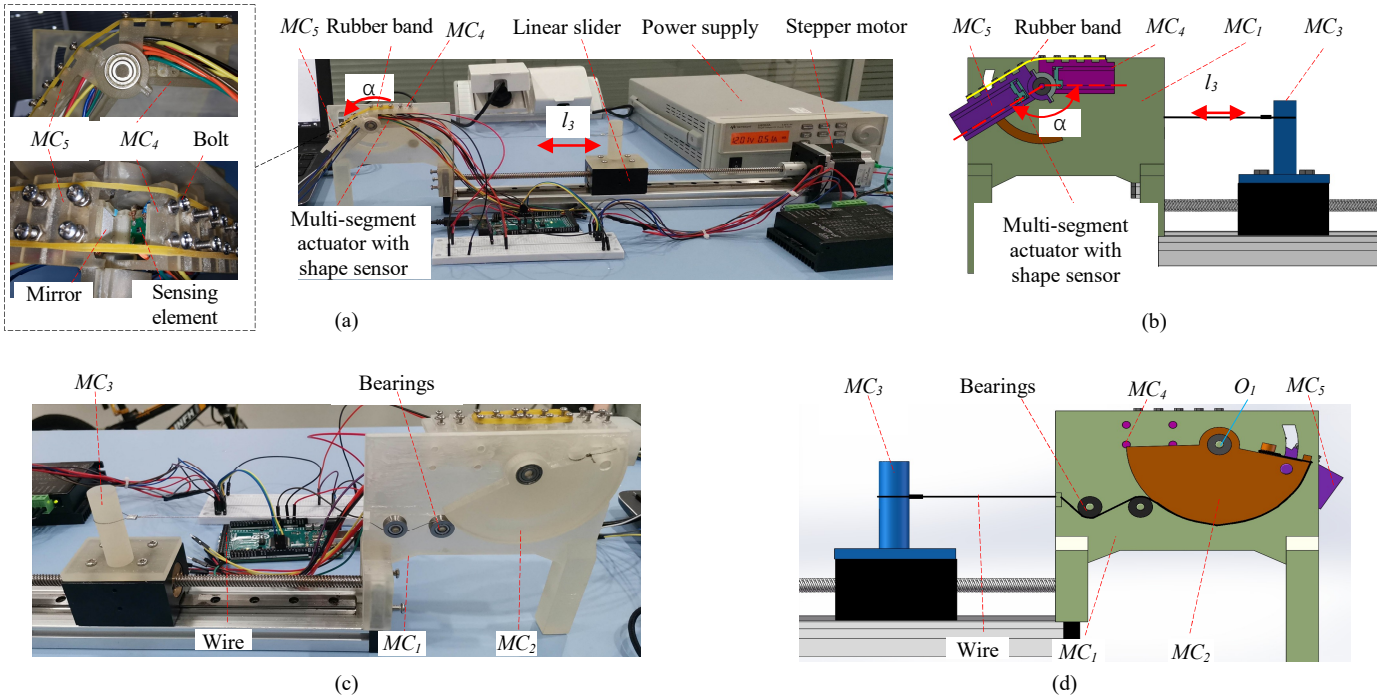
FIGURE 6. Calibration device. (a) and (c) show the calibration device from different angles. (a) left shows the assembly relation among MC_4, MC_5 and the multi-segment actuator with shape sensor. (b) and (d) show the main components with CAD images.

segments to be quickly removed and mounted with bolts.

The moving slider, through the wire and MC_2, drives MC_5 to realize precise clockwise rotation (as shown by the red arrow in Fig. 6(a) and (b)). A rubber band provides the power for the anti-clockwise rotation to MC_5. The relationship between stepper motor travel distance l_3 and the rotation angle of MC_5 relative to MC_4 (α) is expressed using (3).

$$l_3 = \alpha \pi r / 180 \qquad (3)$$

B. Calibration Experiments And Analysis of Results

The five sensing elements integrated into the adjacent small segments were calibrated in sequence. In the calibration experiments, the operating stroke of the stepper motor was 70 mm, and the rotation angle of MC_5 was calculated at 89.13°. The stepper motor drove MC_5 to turn clockwise from 0 to 89.13° and back to 0. The output voltage of the sensing elements was recorded for every 0.1 mm displacement of the linear slider (every 0.127° of MC_5 rotation). Testing of each sensing element was repeated three times.

The relationship between the input rotation angle (θ_i) and the output voltage (U_i) for each sensing elements was calculated using (4). The results are shown in Fig. 7. Table I shows the characteristics of each sensing element.

$$\theta_i = p_1 * U_i^4 + p_2 * U_i^3 + p_3 * U_i^2 + p_4 * U_i + p_5 \qquad (4)$$

The results indicate that the proposed sensing elements have good sensitivity, satisfactory hysteresis, and high repeatability after being assembled on the target actuator, inline with the design requirements stated in Section II, part A. The clearances of the stepper motor and rubber bands without adequate elasticity may be responsible for the hysteresis errors, which could be improved by replacing the rubber band with a torsion spring. Vibrations of the motor during operation may also

affect the repeatability of the sensor. In the calibration experiment, the output voltage was recorded for every 0.127° of the input rotation angles, which was suitable for the detection of rehabilitation exercises [35]. By enlarging the radius of the MC_2 and improving the sampling frequency (e.g., recording one output voltage point per 0.01 mm of the linear slider motion), the sampling resolution of the calibration device could be enhanced.
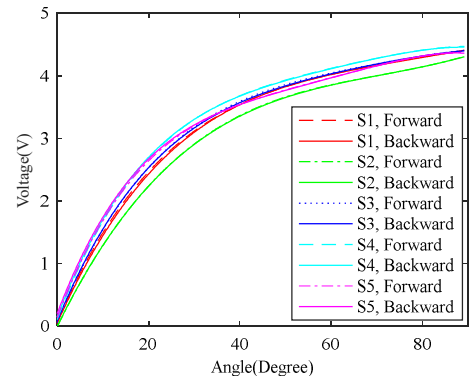

FIGURE 7. Performance of the five sensing elements. In this figure, S1 represents the sensing element 1, S2 represents the sensing element 2, and so on. Forward refers to the results when MC_5 rotates clockwise; backward refers to the results in the other direction.

TABLE I
CHARACTERISTICS OF THE CALCULATED SENSING ELEMENTS

	Sensitivity (V/°)	Hysteresis error	Repeatability error
Sensing element 1	0.0486	0.24%	1.68%
Sensing element 2	0.0487	1.06%	1.78%
Sensing element 3	0.0489	1.07%	0.79%
Sensing element 4	0.0491	0.29%	1.00%
Sensing element 5	0.0477	0.24%	0.57%

C. Benchmarking Using an Off-The-Shelf Sensing System

The usefulness of the sensor unit was verified by comparing the sensor unit's output (θ) with the PIPJ motion angle (δ) of a wooden hand model. The setup is shown in Fig. 8(a). The sensor unit was integrated into the actuator structure corresponding to the PIPJ; θ was calculated by the results of sensing elements calibration, and (1); The PIPJ motion angle was measured by the VICON T40s motion capture system in a static laboratory environment with a mean precision of 0.046 mm [36]. Three markers were separately attached to the proximal phalanx, PIPJ, and the media phalanx, and were marked as M_1, M_2, and M_3. Tracing the spatial position of the three markers yielded a triangle consisting of points M_1, M_2, and M_3, and δ could be obtained by calculating the interior angle of this triangle.

Before the experiment, the actuator was attached to the PIPJ joint with a thin wire. During the experiment, the proximal
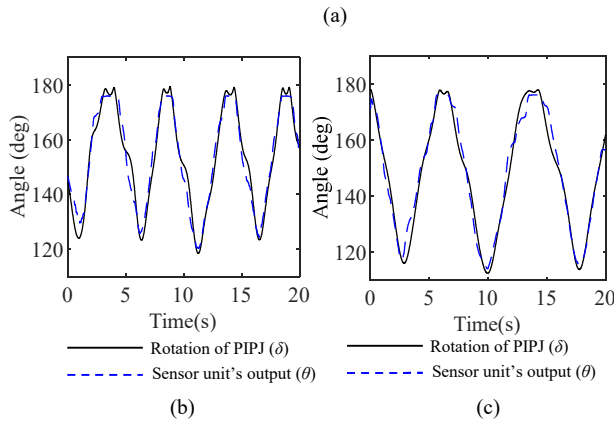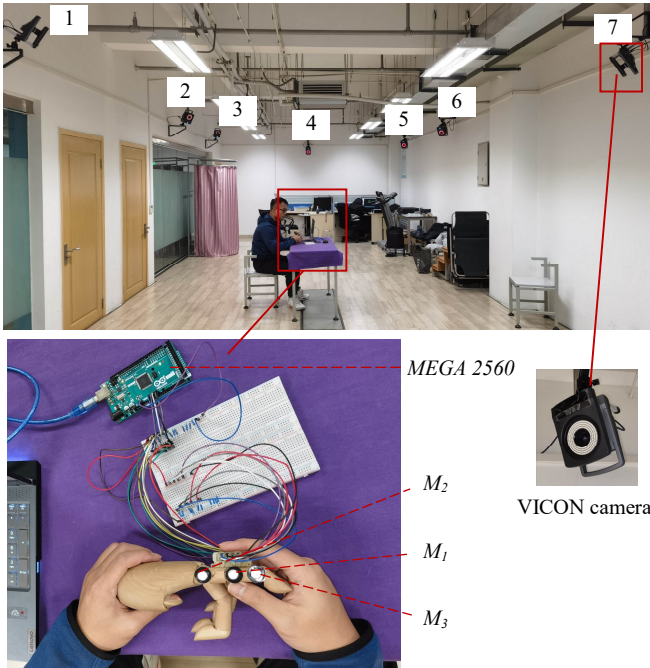
phalanx remained stationary. We pinched the distal interphalangeal joint to assist the media phalanx in rotating around the PIPJ. The designed sensor unit and VICON capture system recorded the actuator bending angle and rotation angle of the media phalanx, respectively, for 20 seconds as one trial and two trials were performed for the validation of the designed sensor unit. Fig.8 (b) and (c) illustrate the results of the repeated two trials.

D. Discussion

Comparing the difference between θ and δ reveals that the sensor unit could measure the actuator bending angle with a mean error of 3.23° and a maximum error of 10.76°. The results prove that the designed sensor unit can be used to monitor the shape of the multi-segment continuous structure. To improve the maximum error to improve clinical feasibility, future work will include the introduction of filtering circuits and other measures.

We employed Dupont wires to connect sensing elements and resisters in this study. As shown in Fig.8(a), the motion of the actuator is affected during the experiment due to the large volume of the Dupont wires. This may also be a result of measurement error. In the next stage, we will focus on the following methods to enhance the flexibility and miniaturization of the sensing system: (1) soldering the sensing elements and resisters onto a flexible PCB to eliminate Dupont wires; (2) replacing color ring resisters with surface-mounted resisters to make the sensor unit compact; (3) optimizing the shape of the flexible PCB to fit more tightly into the actuator; (4) developing a data acquisition system based on the Inter-Integrated Circuit Bus and DA converters.

Table II lists several typical measurement methods or commercial devices for finger movement monitoring. Higher

(a)

(b)   (c)

FIGURE 8. **(a) The verification experimental setup. The actuator bending angle is measured by the designed sensor, and the PIPJ motion angle is measured by the VICON T40S capture system through three markers labeled as M_1, M_2 and M_3; (b) and (c) are the comparison results of two repeated verification trials.**

TABLE II
EXISTING SENSOR MONITORING METHODS FOR POSTURE MONITORING

Reference number	Sensing method	Performance	Other Features
[37]	Resistance	Range: 60K - 110KΩ; Tolerance: ±30%	Price: $16
[38]	VICON	Accuracy<0.3mm	Expensive, and need markers
[39]	Data Glove	22 columns Accuracy:1° Repeatability:3°	Expensive, high precision
[40]	Motor encoder	512 counts per revolution; Resolution:0.007 mm	Difficult to assemble in the multi-segment structure
[41]	Flexible Strain sensor	Sensitivity : 0.31 kPa^{-1}; Repeatability:1.3%; Hysteresis : 4.49%; Durability:10000 cycles; Response time: 20ms;	Large measuring range; detection of physiological signal acoustic vibrations and hand motion
Our sensor	Photo-electric	Sensitivity>0.047 V/°; Repeatability<1.8%; Hysteresis<1.1%; Durability>10000 cycles	Low-cost, small size and detection of different curvatures and shapes.

precision measurement methods such as VICON, Data Glove, Motor encoder etc. will significantly increase the cost of the entire device and make it difficult to integrate with the target exoskeleton. Flexible sensors can be integrated more effectively in exoskeletons for gesture recognition with high flexibility. Compared with the flexible sensor proposed in [41], our sensor has similar durability as well as repeatability and a smaller hysteresis error.

The advantages of the proposed sensor are as follows: 1) Great generalization ability. The sensor unit could be widely applicable to other robot applications, such as continuous soft robot grippers, soft exoskeletons, and soft prosthetics. In these applications, the curvature of the actuator is not constant, and their shape depends on the object they are grabbing. This sensor unit might be utilized to detect different curvatures and then reconstruct the corresponding surface shapes. 2) Potential as a small size and optoelectronic measurement mechanism. The sensor unit has the potential to integrate with the multi-segment continuous structure without affecting its motion. Compared with the flexible strain sensor, the non-deformation property ensures the accuracy and durability of the sensor. 3) User-friendly. The simple and low-cost measuring circuit in this sensor helps to overcome the difficulty of shape monitoring for continuous actuators. This friendly design would be enlightening for those researches related to shape monitoring of rehabilitation exoskeletons.

V. Conclusion And Futures Works

In this proof-of-concept paper, a shape sensor unit consisting of five sensing elements was proposed for measuring the bending angle of a multi-segment continuous structure based on the principle of reflective photoelectric sensing. An easy-to-install calibration device was designed and fabricated for precise calibration of the sensing elements after being integrated into the target actuator. The calibration results showed that these sensing elements had a sensitivity of more than 0.047 V/°, a hysteresis below 1.1%, and a repeatability error below 1.8%. In addition, the output of the designed sensor unit was compared with the detection results of the VICON system to verify the performance of the sensor unit. The result showed that the sensor unit had a mean error of 3.23° and a maximum error of 10.7° for angle detection.

In future studies, flexible PCB will be employed to make the sensing system more flexible and miniaturized to be integrated into the actuator without affecting the movement. The designed sensor unit will also be assembled on all the joints of our exoskeleton to monitor exoskeleton movement and improve exoskeleton position control. The safety mechanism based on the proposed pose monitoring method in this paper will be integrated into the exoskeleton control system. Additionally, a shell that encloses the actuator will be designed to protect the mirror's properties and to block ambient light from affecting the sensor results.

References

[1]   P. Heo, *et al.*, "Current hand exoskeleton technologies for rehabilitation and assistive engineering," *International Journal of Precision Engineering and Manufacturing,* vol. 13, pp. 807-824, 2012.

[2]   C. D. Takahashi, *et al.*, "Robot-based hand motor therapy after stroke," *Brain,* vol. 131, pp. 425-437, 2008-02-01 2008.

[3]   S. Ueki, *et al.*, "Development of a Hand-Assist Robot With Multi-Degrees-of-Freedom for Rehabilitation Therapy," *IEEE/ASME Transactions on Mechatronics,* vol. 17, pp. 136-146, 2012.

[4]   M. Li, *et al.*, "An Attention-Controlled Hand Exoskeleton for the Rehabilitation of Finger Extension and Flexion Using a Rigid-Soft Combined Mechanism," *Frontiers in Neurorobotics,* vol. 13, May. 2019.

[5]   Donghyun Sim, *et al*, "Low-Latency Haptic Open Glove for Immersive Virtual Reality Interaction," *Sensors,* vol. 21, pp. 1-21, 2021.

[6]   A. de Los Reyes-Guzmán, *et al*, "Quantitative assessment based on kinematic measures of functional impairments during upper extremity movements: A review," *Clinical Biomechanics,* vol. 29, pp. 719-727, 2014.

[7]   N. Yang, *et al*, "Motion quality evaluation of upper limb target-reaching movements," *Medical engineering & physics,* vol. 24, pp. 115-120, Jan. 2002.

[8]   F. Saunders, *et al*, "Experimental verification of soft-robot gaits evolved using a lumped dynamic model," *Robotica,* vol. 29, pp. 823-830, 2011.

[9]   H. Hsiao, J. S. Higginson and S. A. Binder-Macleod, "Baseline predictors of treatment gains in peak propulsive force in individuals poststroke," *Journal of NeuroEngineering and Rehabilitation,* vol. 13, 2016.

[10] S. G. Seo, *et al*, "Repeatability of a multi-segment foot model with a 15-marker set in healthy adults," *J Foot Ankle Res,* vol. 7, p. 24, Jan. 2014.

[11] S. Kim, S. Park and O. Lee, "Development of a Diagnosis and Evaluation System for Hemiplegic Patients Post-Stroke Based on Motion Recognition Tracking and Analysis of Wrist Joint Kinematics," *Sensors,* vol. 20, p. 4548, Aug. 2020.

[12] G. Du, *et al*, "Natural Human–Machine Interface With Gesture Tracking and Cartesian Platform for Contactless Electromagnetic Force Feedback," *IEEE Transactions on Industrial Informatics,* vol. 16, pp. 6868-6879, 2020.

[13] L. Wang, J. Liu and J. Lan, "Feature Evaluation of Upper Limb Exercise Rehabilitation Interactive System Based on Kinect," *IEEE Access,* vol. 7, pp. 165985-165996, 2019.

[14] C. D. Metcalf, *et al*, "Markerless Motion Capture and Measurement of Hand Kinematics: Validation and Application to Home-Based Upper Limb Rehabilitation," *IEEE Transactions on Biomedical Engineering,* vol. 60, pp. 2184-2192, 2013.

[15] C. A. E. A. Silva A S, "Design and characterizatino of a wearable macrobending fiber optic sensor for human joint angle determination," *Optical Engineering,* vol. 12, 2013.

[16] S. Sareh, *et al*, "Macrobend optical sensing for pose measurement in soft robot arms," *Smart materials and structures,* vol. 24, p. 125024, Jan. 2015.

[17] T. C. Searle, *et al*, "An optical curvature sensor for flexible manipulators," in *2013 IEEE International Conference on Robotics and Automation (ICRA)*, Karlsruhe, Germany, May 6-10, 2013, pp. 4415-4420.

[18] S. Sareh, *et al*, "A 7.5mm Steiner chain fibre-optic system for multi-segment flex sensing," in *2015 IEEE/RSJ International Conference on Intelligent Robots and Systems (lROS),* Hamburg, Germany, 2015, pp. 2336-2341.

[19] M. Lei, *et al*, "Ultrafast FBG Interrogator Based on Time-Stretch Method," *IEEE Photonics Technology Letters,* vol. 28, pp. 778-781, 2016.

[20] M. A. Davis, *et al*, "Shape and vibration mode sensing using a fiber optic Bragg grating array," *Smart materials and structures,* vol. 5, pp. 759-765, Jan. 1996.

[21] M. Perry, *et al*, "High-Speed Interferometric FBG Interrogator With Dynamic and Absolute Wavelength Measurement Capability," *Journal of Lightwave Technology,* vol. 31, pp. 2897-2903, 2013.

[22] M. Majumder, *et al*, "Fibre Bragg gratings in structural health monitoring—Present status and applications," *Sensors and Actuators A: Physical,* vol. 147, pp. 150-164, 2008.

[23] M. Anwar Zawawi, S. O'Keffe and E. Lewis, "Intensity‐modulated fiber optic sensor for health monitoring applications: a comparative review," *Sensor Review,* vol. 33, pp. 57-67, Jan. 2013.

[24] M. Li, *et al*, "Model-Free Control for Continuum Robots Based on an Adaptive Kalman Filter," *IEEE/ASME Transactions on Mechatronics,* vol. 23, pp. 286-297, 2018.

[25] M. Mahvash and P. E. Dupont, "Stiffness Control of Surgical Continuum

Manipulators," *IEEE Transactions on Robotics,* vol. 27, pp. 334-345, 2011.

[26] M. Melzer, *et al*, "Wearable magnetic field sensors for flexible electronics," *Adv Mater,* vol. 27, pp. 1274-80, Feb. 2015.

[27] Xiang Fu, et al, " Stretchable strain sensor facilely fabricated based on multi-wall carbon nanotube composites with excellent performance," *Journal of Materials Science*, vol. 54, pp. 2170-2180, 2019.

[28] M. Amjadi, *et al*, "Stretchable, Skin-Mountable, and Wearable Strain Sensors and Their Potential Applications: A Review," *Advanced Functional Materials,* vol. 26, pp. 1678-1698, 2016.

[29] T. Yamada, *et al*, "A stretchable carbon nanotube strain sensor for human-motion detection," *Nature Nanotechnology,* vol. 6, pp. 296-301, 2011.

[30] Y. Li, *et al*, "Highly Flexible Strain Sensor from Tissue Paper for Wearable Electronics," *ACS sustainable chemistry & engineering,* vol. 4, pp. 4288-4295, Jan. 2016.

[31] S. Yao and Y. Zhu, "Wearable multifunctional sensors using printed stretchable conductors made of silver nanowires," *Nanoscale,* vol. 6, p. 2345, 2014.

[32] K. J. Benjamin, *et al*, "Optoelectronic Sensor-based Shape Sensing Approach for Flexible Manipulators," in *2019 41st Annual International Conference of the IEEE Engineering in Medicine and Biology Society (EMBC)*, Berlin, Germany, July 23-27, 2019.

[33] D. Osman, *et al*, "An Optical Joint Angle Measurement Sensor based on an Optoelectronic Sensor for Robot Manipulators," in *2020 8th International Conference on Control, Mechatronics and Automation (ICCMA),* Moscow, Russia, Nov. 6-8, 2020.

[34] M. K. Dobrzynski, R. Pericet-Camara and D. Floreano, "Contactless deflection sensor for soft robots," in *2011 IEEE/RSJ International Conference on Intelligent Robots and Systems,* San Francisco, CA, USA, Sept. 25-30, 2011.

[35] J. E. Nitschke, *et al*, "Reliability of the American Medical Association Guides' Model for measuring Spinal Rang of Motion," *Spine,* vol. 3, pp. 262-268, 1999.

[36] S. L. Raghu, *et al*, "Static accuracy analysis of Vicon T40s motion capture cameras arranged externally for motion capture in constrained aquatic environments," *Journal of Biomechanics,* vol. 89, pp. 139-142, 2019.

[37] V. Durairajah, *et al*, "Design and Development of Low Cost Hand Exoskeleton for Rehabilitation," in *2nd International Conference for Innovation in Biomedical Engineering and Life Sciences,* Singapore, 2017.

[38] I. Carpinella, J. Jonsdottir and M. Ferrarin1, " Multi-finger coordination in healthy subjects and stroke patients: a mathematical modelling approach," *Journal of NeuroEngineering and Rehabilitation,* pp. 8-19, 2011.

[39] M. Atzori, *et al*, "Electromyography data for non-invasive naturally-controlled robotic hand prostheses," *Scientific Data*, 2014.

[40] C. G. Rose and M. K. O'Malley, "Hybrid Rigid-Soft Hand Exoskeleton to Assist Functional Dexterity," *IEEE ROBOTICS AND AUTOMATION LETTERS,* vol. 4, no. 1, pp. 73-80, 2019.

[41] K Kim, *et al,* "Robust and scalable three-dimensional spacer textile pressure sensor for human motion detection," *Smart Mater. and Struct.,* 28, pp. 1-8, 2019.

Bo He received his B.S. Degree in Mechanical Engineering from Yanshan University of China in 2016. He is currently a Master's degree candidate in the school of Mechanical Engineering at Xi'an Jiaotong University. His research interests include rehabilitation robot and human motion detection.

Sina Sareh received the B.S. degree in electrical engineering from Tehran Polytechnic, Iran, in 2005, the M.S. degree in control systems from the University of Sheffield, U.K., in 2007, and the Ph.D. degree in robotics from the University of Bristol, U.K., in 2012. Dr Sareh is the Academic Leader in Robotics at Royal College of Art. He is currently a Reader in Robotics and Design Intelligence and a Fellow of the Engineering and Physical Sciences Research Council (EPSRC) whose research develops new robotic solutions to human safety, access and performance issues in medical and industrial operations.
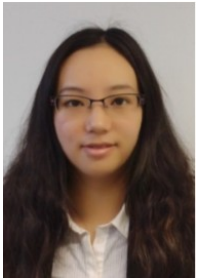
Min Li received her B.Sc. degree in mechanical engineering and her M.Sc. degree in agricultural mechanization engineering from Northwest A&F University, China, in 2007 and 2010, respectively, and the Ph.D. degree in robotics from King's College London in 2014. From 2015 to 2017, she was a Lecturer with the School of Mechanical Engineering, Xi'an Jiaotong University, China. She is currently an Associate Professor with Xi'an Jiaotong University. Her research interests include haptic feedback for robots, soft robots and rehabilitation robots.

Jun Xie received the B. Sc. Degree in mechanical engineering and the M.Sc. degree in fluid machinery and engineering from the Hefei University of Technology, China, in 2004 and 2007, respectively, and the Ph.D. degree in instrument science and technology from Xi'an Jiaotong University, China, in 2013. Since 2017, he has been an Associate Professor with the School of Mechanical Engineering, Xi'an Jiaotong University. His research interests include brain signal processing and brain–computer interface.

Renghao Liang, Ph.D, State Key Laboratory for Manufacturing Systems Engineering Mechanical Engineering college, Xi'an Jiaotong University, China. His current research directions are involving rehabilitation exoskeletons, topology optimization for compliant mechanisms and bionic exoskeletons.

Guanghua Xu received the B.Sc. and M.Sc. degrees and the Ph.D. degree in mechanical engineering from Xi'an Jiaotong University, Xi'an, China, in 1986 and 1995, respectively. He is current a Professor of Mechanical Engineering with Xi'an Jiaotong University. His research interests include biomedical signal processing, brain–computer interface, rehabilitation robot, and condition monitoring and fault diagnosis.

Ziting Liang received the B.S. degree in mechatronic engineering from the Qinghai University, China in 2018. He is currently pursuing the master's degree with the School of Mechanical Engineering, Xi'an Jiaotong University. His research interests include rehabilitation robotics and brain-computer interface.

Yohan Noh received the B.S. degree from the Department of Mechanical Engineering, Seoul National University of Science and Technology, South Korea, in 2002, the B.S. degree from the Department of Electrical Engineering, Yonsei University, South Korea, in 2004, and the M.S. and Ph.D. degrees from the Department of Science and Engineering, Waseda University, Tokyo, Japan, in 2007 and 2011, respectively. He worked as a Research Associate for Robotics Research in the Department of Biomedical Engineering, King's College London 2013 to 2019. Currently, he is working as a lecturer in the Department of Mechanical and Aerospace Engineering, Brunel University London. His research interests include development of force and tactile sensors, haptics, robot assisted ultrasound diagnostic system, medical training system, and medical robots.

Wei Yao received the Ph.D. degree in robotics in 2007. Previously, he was a Postdoc Research Fellow at King's College London for a project of developing an MRI compatible steerable robotic catheter system for cardiac catheterization. Before he moved to King's College, he worked for two years in the Department of Surgery and Cancer at Imperial College London, carrying on research into robotics for minimally invasive surgery. Currently, he is a Lecturer in medical robotics in the Department of Biomedical Engineering, University of Strathclyde, Glasgow, U.K. His research focuses on developing a number of cutting-edge and multi-discipline robotic technologies by integrating mechatronics, sensing, control, medical imaging and robotic navigation for the next generation of surgery and rehabilitation.